This paper appears in Biomedical Signal Processing and Control
https://doi.org/10.1016/j.bspc.2021.102423

Neural Network-Based Physiological Organ Motion Prediction and Robot Impedance Control for Teleoperated Beating-Heart Surgery

Lingbo Cheng[1,2*] and Mahdi Tavakoli[2]

[1]*College of Control Science and Engineering, Zhejiang University, Hangzhou, Zhejiang, 310027 China*

[2]*Department of Electrical and Computer Engineering, University of Alberta, Edmonton, AB, T6G 1H9 Canada*

Abstract

Compared to conventional arrested heart surgery, beating-heart surgery is promising as the advantages of eliminating adverse effects caused by a heart-lung bypass machine and enabling intraoperative evaluation of heart motion. However, the fast motion of the heart introduces a significant challenge for beating-heart surgery. In this paper, a teleoperation system, which employs an impedance control for the master robot and an ultrasound image-based position control for the slave robot (surgical robot), is proposed to achieve non-oscillatory force feedback and heart motion compensation, respectively. Specifically, an impedance model is designed for the master robot to provide the human operator (surgeon) with non-oscillatory haptic feedback. To compensate for the beating heart's motion, ultrasound imaging is used to obtain the position of the point of interest (POI) on the heart tissue. As the use of ultrasound imaging introduces non-negligible time delay caused by image acquisition and processing, a recurrent neural network (NN)-based physiological organ motion predictor is proposed. The predicted POI position is used to control the slave robot to automatically compensate for the beating heart's motion. The proposed method is validated through experiments. The proposed control strategy with NN-based heart motion predictor is compared to the other two strategies without heart motion predictor and with an extended Kalman filter (EKF)-based heart motion predictor. The experimental results present that the proposed strategy with NN algorithm shows significant advantages (higher synchronization accuracy and relatively steady slave-heart contact force) over the other two strategies.

Keywords

Ultrasound image, neural network, motion compensation, teleoperation system, medical robotics.

1 Introduction

Cardiovascular disease is one of the leading causes of death worldwide [1]. Conventional heart surgery requires the heart is arrested by connecting the patient to a heart-lung bypass machine, which has the same function as a beating heart to provide blood and oxygen to the patient's body. However, the use of heart-lung bypass machine introduces adverse effects [2]–[6] to the patients such as the increased risk of stroke and possible long-time cognitive loss [2], [7]. Moreover, for arrested-heart surgery, it is difficult to evaluate the heart motion during operation; that is, the evaluation of the heart motion can only be implemented after the heart beats normally again [8]. On the contrary, beating-heart surgery can eliminate such negative effects by allowing the heart to beat normally. For beating-heart surgery, the most prominent challenge needs to be addressed is the rapid movement of the beating heart, whose movement velocity and acceleration are approximately 210 mm/s and 3800 mm/s^2, respectively [9].

In clinical practice, a heart stabilizer [10] is generally used to hold a small area tissue on the surface of the beating heart to keep the tissue from moving. However, this heart stabilizer can only be used for extracardiac surgery and the heart movement cannot be eliminated completely. To date, to compensate for the beating heart's motion, robot-assisted beating-heart surgery has been proposed by employing a surgical robot and synchronizing its motion with the beating heart's motion via position and/or force control. By automatically synchronizing the surgical robot position with the beating heart's motion, the position commands exerted by the human operator will be executed on a seemingly arrested heart. In fact, the summed position of the human operator and the heart will act as the reference value for the surgical robot. This can improve the precision and accuracy of beating heart surgical procedures and decrease the fatigue and exhaustion of the human operator.

For robot-assisted beating-heart surgery, a teleoperation system offers more advantages over a hand-held device for surgery, especially in minimally invasive surgery [11], such as more accuracy and repeatability, the facilitation of motion scaling, and the ability to telemanipulate the surgical robot over a long distance. A master-slave teleoperation system generally involves a master robot that provides position commands and a slave robot that receives those commands and executes tasks on the heart tissue. The human operator will manipulate the master robot to implement tasks instead of directly operating on the heart tissue. As the surgical robot will follow the master robot's position commands, it is defined as the slave robot in a telerobotic system. To guarantee the human operator to feel the interaction force between the slave robot and the beating-heart tissue, a bilateral teleoperation system (haptic feedback) is necessary. With haptic feedback, both accuracy and repeatability of the forces can be improved [12], and tissue damages and undesirable trauma can be reduced [13]. Therefore, in this paper, we will focus on a bilateral teleoperation system for beating-heart surgery.

*Corresponding Author. E-mails: lingbo1@ualberta.ca; phone: 780-492-8935.

An essential issue for the bilateral teleoperation system is the non-oscillatory haptic feedback. To avoid the induced motion phenomenon [14], the human operator should only feel a force that one would feel when directly working on an arrested heart. In other words, the quasi-periodic heartbeat-induced forces caused by the residual position mismatch between the slave robot and the heart motion and by the slave-mounted force sensor's internal inertia should not be transmitted to the human operator. Therefore, the oscillatory portion of the slave-heart interaction force should be filtered out [15], and only the non-oscillatory portion should be transmitted to the human operator.

To achieve heart motion compensation and non-oscillatory force feedback, various methods have been proposed. In [16], Nakamura et al. adopt a monochrome high-speed camera to measure the heart position, so that the surgical robot can automatically track a laser-lit point on the heart. In [17], Ginhoux et al. measured the cardiac motions by using a 500-Hz camera to avoid aliasing. In [18], a pair of X-ray cameras and an infrared tracking system were combined to obtain the positions of the internal markers attached to the heart tissue. Another common sensor used for guiding intracardiac beating-heart repairs is the ultrasound machine. Yuen et al. developed an ultrasound-guided motion compensation system for beating-heart mitral valve repair [19], [20]. Kesner et al. applied a robotic catheter system combining ultrasound guidance and force control to perform cardiac tissue ablation [21]. In [22]–[25], the authors developed a teleoperation system and combined ultrasound images with various controllers to compensate for the heart's motion.

In addition to image-based sensors, non-image-based sensors such as force sensors and sonomicrometry crystals are proposed to solve the problem of motion compensation and/or haptic feedback. In [26], [27], the authors utilized force sensors to compensate for the physiological motion by controlling the contact forces to track the desired ones. These methods were assumed that the surgical robot has somehow been initially controlled to contact with the heart, and the control goals are maintaining contact between the tool and the tissue. In [28], [29], the authors used sonomicrometry crystals to track the beating-heart motion in real-time and generalized adaptive predictors to predict the heart's motion. This technique is feasible as the heart position can be captured through blood, although the calculation is complex and time-consuming.

As discussed above, most successful applications of robot-assisted surgical systems have been performed based on position and/or force control; that is, the surgical robot is treated as an isolated system. However, for surgical procedures, control of the dynamic behavior between the surgical robot and the heart tissue is also required. To regulate this kind of dynamic behavior, in our previous research [30]–[32], robot impedance control was used. By designing two reference impedance models for the master and slave robots and appropriately adjusting the parameters of the models, both heart motion compensation and non-oscillatory force feedback could be achieved.

In [25], the master robot impedance control was combined with the ultrasound image-based position control to achieve the system's objectives and extend the application of the systems in [30], [31]. Specifically, the position of the beating heart can be obtained from ultrasound images and be used to synchronize the surgical robot's motion with the heart's motion. However, the time delay caused by ultrasound image acquisition and processing is non-negligible and must be compensated for. Otherwise, the robot will follow the delayed heart motions, which creates the risk of tool-tissue collision and puncture.

To compensate for the time delay, the delayed heart position should be predicted. The heart motion prediction is a problem of time series forecasting, which requires a model to predict future values of the time series based on its present and previously observed values. To solve time series forecasting problems various methods have been proposed such as Kalman filtering, weighted moving average, and exponential smoothing. As the heart motion is quasi-periodic, in [25], an extended Kalman filter (EKF) was used for motion prediction. To improve the prediction accuracy, in this paper, a neural network (NN)-based heart motion prediction method is proposed. It has been demonstrated that a NN model can approximate any continuous function and it has been successfully used for forecasting of many time series in many applications [33], [34]. Also, NN has the advantage that it can approximate nonlinear functions without any prior information of the data series, which makes it suitable for application of quasi-periodic beating-heart motion prediction.

Much of the past work [35]–[37] on using NN to predict an organ's physiological motion has focused on radiotherapy and the prediction of tumor motion under respiration. For image-guided radiotherapy applications, diagnostic X-ray imaging was used to detect the markers on the tumor. In this paper, ultrasound imaging is used to obtain the heart position and no markers are implanted on the surface of the heart to reduce the harm to the human body and increase the observation accuracy of the heart position.

A recurrent NN, which includes feedback loops having a profound positive impact on the learning capability and on the prediction performance, is used in the paper. In our previous research [38], a NN-based heart motion predictor was proposed and compared to an EKF heart motion predictor. And the experimental results show that the NN predictor has significant advantages such as higher prediction accuracy and longer prediction horizon compared to the EKF predictor.

The rest of the paper is organized as follows. Section 2 introduces the developed teleoperation system for beating-heart surgery. Section 3 presents the master robot impedance control method for non-oscillatory haptic feedback to the human operator. Section 4 describes ultrasound image-based heart motion compensation algorithms for the slave robot and NN-based heart motion predictor. Section 5 shows the experimental results of the developed teleoperation system and compares the results of using no predictor, EKF algorithm, and NN algorithm. Finally, Section 6 gives concluding remarks of the paper.

2 Teleoperation System for Beating-Heart Surgery

In the paper, a bilateral teleoperation system is proposed by combining the NN-based heart motion predictor with master robot impedance control. Specifically, to simultaneously achieve non-oscillatory haptic feedback on the master robot and motion compensation for the slave robot, an impedance controller for the master robot and an ultrasound image-based position controller for the slave robot are proposed for telerobotic beating-heart surgery (Figure 1). As will be discussed later, a reference impedance model is designed for the master robot to provide the human operator with the non-oscillatory haptic feedback. The ultrasound imaging is used to obtain the beating heart's position, which is added to the master robot position. The summed position is the reference trajectory for the salve robot so that it can comply with the beating heart's motion and follow the position commands of the human operator. To deal with the time delay caused by ultrasound image acquisition and processing, a recurrent NN is utilized as a heart motion predictor.

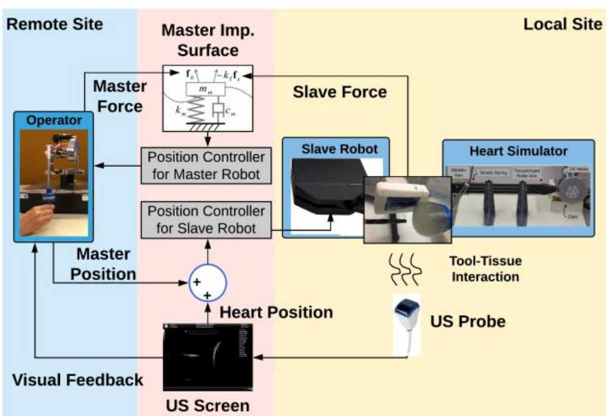

Figure 1. System concept of the proposal. The reference impedance model for the master robot is proposed to provide the human operator with non-oscillatory haptic feedback, and ultrasound imaging is used to obtain the beating heart's position and control the slave robot to synchronize its motion with the fast heart motion.

The developed teleoperation system for beating-heart surgery, which consists of the human operator, the beating heart, the master robot, and the slave robot, is shown in Figure 2. The human operator manipulates the master robot to control the slave robot implement specific surgical task on the beating heart. The objectives of the system are (a) providing non-oscillatory force feedback to the human operator through the master robot, and (b) synchronizing the slave robot with the motion of the beating heart and meanwhile manipulating the slave robot to follow the position commands of the human operator. To this end, two force/torque sensors and an ultrasound machine are used to acquire force and position signals of the robots.

For the master site, to guarantee the human operator mostly perceives the slave-heart interaction forces with little feedback from the oscillatory forces, a reference impedance model is designed for the master robot with appropriate adjusted parameters. In Figure 2, the reference impedance model is related to the interaction force between the human operator and the master robot $\mathbf{f}_h$ and the interaction force between the heart tissue and the slave robot $\mathbf{f}_e$. As will be discussed later, this reference impedance model can filter out the high-frequency portion of $\mathbf{f}_e$ and achieve $\mathbf{f}_h$ equals the filtered $\mathbf{f}_e$, so that the human operator perceives non-oscillatory force feedback. The reference impedance model generates a reference position $\mathbf{x}_{ref_m}$ to the master robot controller for the master robot to follow.

For the slave site, to synchronize the slave robot with the beating heart's motion, an ultrasound machine is used to obtain the position of the beating heart $\mathbf{x}_e$. Through ultrasound image acquisition and processing, the obtained heart position $\mathbf{x}_e$ is added to the position of the master robot $\mathbf{x}_m$, and the summation $\mathbf{x}_r\ (=\mathbf{x}_m+\mathbf{x}_e)$ is transmitted to the slave robot controller as a reference position signal. Therefore, the position of the slave robot $\mathbf{x}_s$ can compensate for the heart's motion and follow the position commands of the master robot.

The presence of ultrasound imaging introduces two challenging issues to be addressed: time delay and slow sampling rate. First, the time delay caused by ultrasound image acquisition and processing is approximate 160 ms, which is not negligible and must be compensated for. Second, the ultrasound machines have slow frame rates typically between 20 to 60 Hz. The robots, however, are controlled at a fast sampling rate, which is 1000 Hz. To unify the sampling rate of the system, the position data collected at the low sampling rate of the ultrasound images should be upsampled.

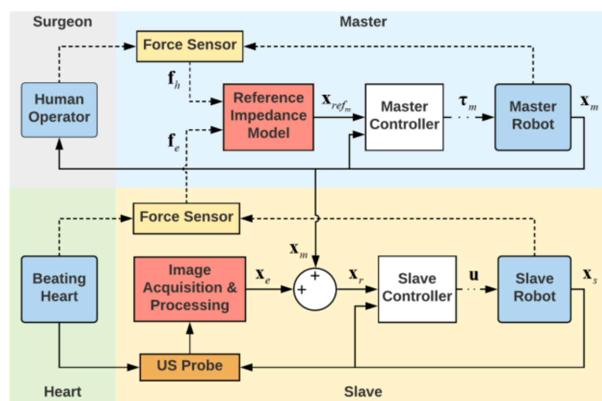

Figure 2. The telerobotic beating-heart surgical system with robot impedance-controlled force feedback and ultrasound image-based motion compensation.

3 Master Robot Impedance Control

The reference impedance model for the master robot includes the interaction force between the human operator and the master robot, $\mathbf{f}_h$, the interaction force between the heart tissue and the slave robot, $\mathbf{f}_e$, and the desired master response trajectory $\mathbf{x}_{ref_m}$. The relationships can be expressed as

$$m_m \ddot{\mathbf{x}}_{ref_m} + c_m \dot{\mathbf{x}}_{ref_m} + k_m \mathbf{x}_{ref_m} = \mathbf{f}_h - k_f \mathbf{f}_e \qquad (1)$$

where k_m, c_m, m_m are the virtual stiffness, damping and mass parameters of the master impedance model. The impedance parameters are set as positive so that the reference impedance model is a stable second-order differential equation. Also, k_f is the force scaling factor.

The transfer function of the reference impedance model for the master robot (1) can be written as a second-order function with a natural frequency ω_{n_m} and a damping ratio ζ_m

$$Z_m = \frac{1}{m_m s^2 + c_m s + k_m} = \frac{\omega_{n_m}^2}{k_m(s^2 + 2\zeta_m \omega_{n_m} s + \omega_{n_m}^2)} \qquad (2)$$

where $\omega_{n_m} = \sqrt{k_m/m_m}$ and $\zeta_m = c_m/2\sqrt{m_m k_m}$. In the following, only k_m, ω_{n_m}, and ζ_m will be adjusted. The virtual mass m_m and damping c_m can be calculated through the three adjusted parameters.

The reference impedance model for the master robot should be designed to provide the human operator with non-oscillatory force feedback. In other words, the model should achieve ($\mathbf{f}_h - k_f \mathbf{f}_e$)→0 when the high frequency of the slave-heart interaction force ($\mathbf{f}_e$) has been filtered to avoid possible exhaustion caused by the reflection of the oscillatory slave-heart interaction force to the human operator. Specifically, the slave-heart interaction force ($\mathbf{f}_e$) is quasi-periodic heartbeat-induced force due to the residual position mismatch between the slave robot and the heart motion and by the slave-mounted force sensor's internal inertia should not be transmitted to the human operator. Therefore, direct force reflection of the oscillatory force $\mathbf{f}_e$ may lead to exhaustion and increased operation difficulties to the human operator. The goal of the reference impedance model for the master robot is to filter out the high-frequency portion of $\mathbf{f}_e$ and achieve ($\mathbf{f}_h - k_f \mathbf{f}_e^l$)→0 ($\mathbf{f}_e^l$ is the low-frequency portion of $\mathbf{f}_e$).

To this end, the natural frequency of the reference impedance model for the master robot, ω_{n_m}, should be much lower than that of the beating-heart, ω_{n_H}, which has a range of 6.28 ~ 10.68 rad/sec. In other words, ω_{n_m} should be a small value ($\omega_{n_m} \leq 0.6$ rad/sec << ω_{n_H}) based on the Bode plot of the second order impedance model (2) [39]. In addition, the stiffness parameter, k_m, of the reference impedance model for the master robot (1) should be chosen to be a small value so that to achieve ($\mathbf{f}_h - k_f \mathbf{f}_e^l$)→0. To make the system have a fast behavior in response to the harmonic physiological force of the human operator, the damping ratio of the impedance model (2) (ζ_m) is chosen to be 0.7.

To control the position of the master robot $\mathbf{x}_m$ to follow the reference trajectory $\mathbf{x}_{ref_m}$, a proportional-integral-derivative controller (PID controller) is used for the master robot. The parameters of the PID controller for the master robot are K_{p_m} = 1000, K_{i_m} = 200, K_{d_m} = 1.

4 NN-based Heart Motion Compensation

In this section, a NN-based heart motion compensation algorithm is proposed for the slave robot. For the sake of brevity, we assume that the heart movement is a back and forth one degree-of-freedom (DOF) motion. This assumption is reasonable as for some specific cardiac surgeries such as mitral valve annuloplasty the target tissue motion is mainly along the direction of the major component of heart motion [19]. For clinical applications that require multi-DOF heart motions, it can be achieved by adjusting one axis of the slave robot frame along the direction of the major component of heart motion [32].

The objective of the designed heart motion compensation method for the slave robot is to synchronize the slave robot's motion with the fast heart motion and meanwhile control the slave robot to follow the position commands of the human operator. As shown in Figure 3, the desired reference trajectories for the salve robot, x_{ref_s}, is the summation of the beating heart's position, x_e, and the master robot position, x_m. The beating-heart position can be calculated based on the position of the slave robot and the measured robot-heart distance by ultrasound machine along with the surgical tool's axis.

The real-time positions of the master and slave robots are measurable through the end encoders attached to the robots' end-effectors. However, the real-time beating heart's position with the same sampling rate as the system, x_e, is tough to be directly measured due to the non-negligible delay caused by ultrasound image acquisition and processing and the slow sampling rate of the ultrasound machine.

To obtain x_e, four steps are designed as shown in Figure 3. First, the distance between the surgical tooltip and the heart tissue, X_d^d, is detected through image processing algorithms. Second, the delayed beating heart's position with low sampling rate, X_e^d, is obtained by adding the delayed and down-sampled slave robot position, X_s^d, to the robot-heart distance, X_d^d. It is feasible because the direction of the surgical tool attached to the slave robot's end-effector is set the same as the direction of the beating heart. So, the measured robot-heart distance X_d^d can be converted to the slave robot's frame by converting it from pixels into mm. The first two steps can be summarized to *heart motion tracking*.

And then, *heart motion prediction*: the delayed X_e^d is predicted through a NN-based motion predictor to obtain X_e. Finally, *heart motion upsampling*: X_e is upsampled to x_e, which has a high sampling rate. It should be noted that the order of motion prediction and upsampling has no big difference to the system. To reduce computation time, heart motion prediction is put first.

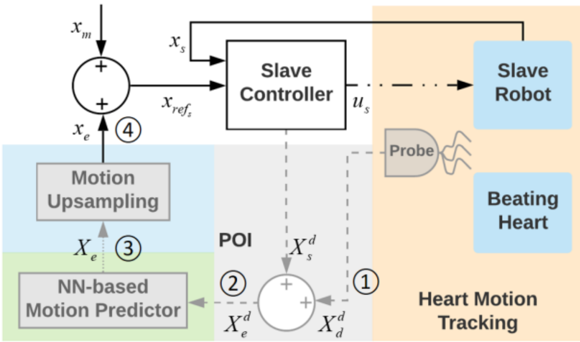

Figure 3. NN-based motion compensation control system. Due to the time delay caused by image acquisition and processing, the system includes two classes of data: real-time data (shown by black lines) and delayed data (shown by gray lines). Here, X_d^d indicates the measured robot-heart distance by ultrasound machine, which is delayed and slowly sampled. Also, X_s^d and X_e^d are the delayed slave robot position and the delayed beating heart position under a slow sampling rate, respectively. The superscript d indicates the data is delayed. The predicted beating heart position with a slow sampling rate using NN predictor is indicated by X_e. In addition, the current heart position, which has both high sampling rate and no delay is indicated by x_e.

4.1 Heart Motion Tracking

The beating-heart motion data can be obtained through ultrasound image acquisition and processing. As the beating-heart motion is assumed to be a back and forth one-DOF movement, for the sake of brevity, a point of interest (POI) on the surface of the heart is employed to represent the position of the beating heart. Specifically, the position of the POI on the beating heart is defined as the heart position along the surgical instrument's axis, and it can be calculated through feature extraction algorithms.

4.1.1 Image Acquisition

The heart simulator employs a one-DOF custom-built mechanical cam and a voice coil actuator (NCC20-18-020-1X from H2W Technologies Inc., Santa Clarita, CA, USA) to simulate the back and forth beating heart's movement (Figure 4). The heart simulator can produce quasi-periodic motion signals, which temporally matched to an ECG signal [40], with a peak-to-peak amplitude of 9 mm. The movement has a fundamental frequency of 7.04 rad/sec, which will be used to adjust the parameters of the reference impedance model for the master robot.

To simulate the heart tissue, an artificial plastisol-based tissue is mounted on the tip of the heart simulator. A straight and rigid tool used as a surgical instrument is mounted on the end-effector of the slave robot. Both the plastic tissue and the rigid tool are submerged in a water tank, which is used to simulate the heart's blood pool and guarantee that both the simulated heart tissue and the rigid tool are visible under the ultrasound. The ultrasound image sequences are acquired through a 6MHz 4dl14-5/38 linear 4D transducer connected to a SonixTouch US scanner (SonixTouch from Ultrasonix, Richmond, BC, Canada) (Figure 4). The 2D US images are collected from the US scanner using a DVI2USB 3.0 frame grabber (Epiphan, Ottawa, ON, Canada). The frame rate of the ultrasound scanner is 25 Hz. The depth of the US images is 5.5 cm.

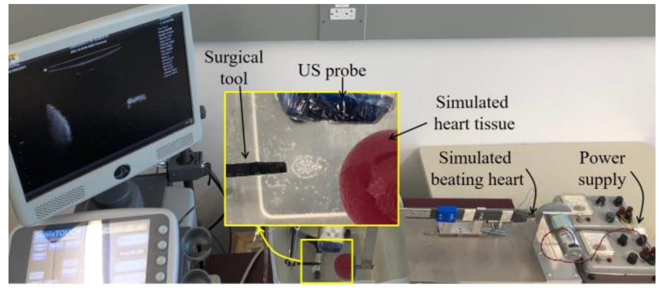

Figure 4. The experimental setup for ultrasound image acquisition.

4.1.2 Image Processing

Through image processing, the slow sampled and delayed robot-heart distance X_d^d can be measured directly from each ultrasound image. For this purpose, as shown in Figure 4, the movement directions of the surgical tool and beating heart are set as the same, and the scanning plane of the ultrasound probe is set to through this direction so that both the surgical tool and the heart tissue surface can be clearly detected in each ultrasound image.

To begin, each original acquired image is converted to black and white by choosing a binary threshold of 0.3. And then, the edge points of each binary image are obtained by a convolution operation with an operator of 3×3 Sobel edge detection algorithm [41]. After that, the longest line, which is the detected surgical tool, in each image is identified by a Hough transform [42]. The extension of the longest line through the surgical tool has an intersection with the surface of the heart tissue, which is defined as the POI on the surface of the heart (Figure 5). The points of surgical tooltip and POI presented in Figure 5 provide the robot-heart distance, X_d^d. For special cases, when the surgical tooltip contacts the heart tissue, the robot-heart distance is assumed to be zero. As the direction of the surgical tool attached to the slave robot's end-effector is set the same as the direction of the beating heart's motion, the measured robot-heart distance X_d^d can be converted to the slave robot's frame by converting it from pixels into mm. By adding the delayed and down-sampled slave robot position, X_s^d, to the robot-heart distance, X_d^d, the delayed beating heart's position with a low sampling rate, X_e^d, is obtained.

To compare the tracked POI position data with the actual position of the simulated beating heart, a potentiometer (LP-75FP-5K from Midori America Corp., Fullerton, CA, USA) is used to collect and record the real-time position of the beating-heart simulator. For this purpose, the surgical instrument (slave robot) is kept still, and the POI position can be acquired directly from the measured tool-heart distance along with the surgical tool's axis. Figure 6 shows the comparison results. The mean absolute error between the tracked data and the directly measured data of a 1000 s-long data is 0.5697 mm, which is 0.0633 of the peak-to-peak amplitude of the heart motion and is sufficiently small.

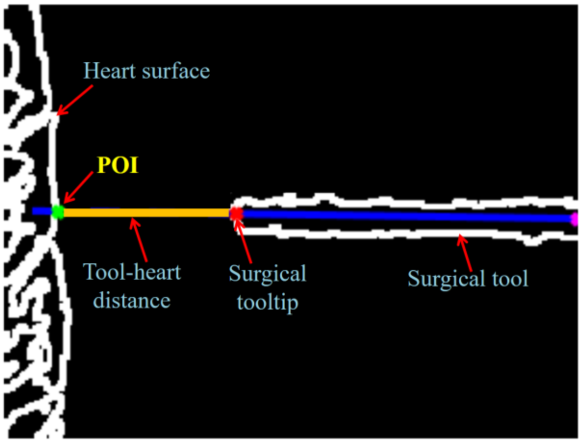

Figure 5. The detected tooltip, POI, and tool-heart distance.

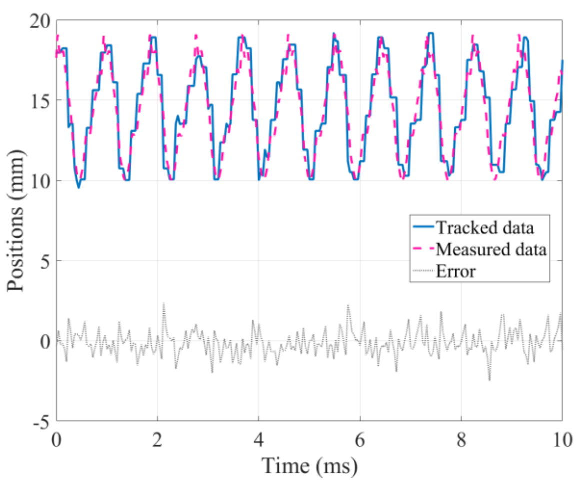

Figure 6. Positions of the tracked and directly measured POI on the surface of the heart.

The tracked POI data is treated as a time series and will be sent to a NN for training and test. Therefore, five ultrasound image sequences each ~ 1000 s long are recorded for the training and test of the NN. The corresponding time series of the tracked POI position data are labelled as dataset 1-5. To implement the NN, the acquired five POI position datasets will be split into training and out-of-sampling test subsets separately. Specifically, the first 75% of each dataset is used for training and the left is reserved for test.

4.2 Heart Motion Prediction

To compensate for the time delay caused by ultrasound image acquisition and processing, a NN-based heart motion predictor is designed. The heart motion prediction problem can be described as given an input vector $\mathbf{x}(n)$, which consists of the current and past heart positions, the NN model must capture the underlying dynamics responsible for generating the next position point, $x(n+1)$. For multiple-step ahead prediction of $x(n)$, namely, to predict $x(n+D)$, where D is the delay length that needs to be compensated for, a closed-loop NN is employed. Therefore, the goals in this section are using training and test datasets to explore the optimal form of the input vector $\mathbf{x}(n)$ and the optimal architecture of the NN. Note that, here $x(n)$ indicates the data point of the delayed heart motion with a slow sampling rate, X_e^d, and $x(n+D)$ indicates the predicted heart position with a slow sampling rate, X_e.

4.2.1 Recurrent NN

A recurrent NN, which has at least one feedback loop, can use its internal memory to process sequences of inputs. As the problem is to predict the quasi-periodic heart motion $x(n)$ which is a time series given the present and past values of $x(n)$, there is no external input to the network, a nonlinear autoregressive (NAR) neural network, therefore, is appropriate to learn and implement the recursive prediction of heart motion.

The architecture layout of a NAR employs a generic recurrent NN that follows naturally from a static multilayer perceptron (MLP) with two hidden layers (Figure 7). The NAR model has a single output that is fed back to the input layer of the MLP via a tapped-delay-line memory of q units. The vector $\mathbf{x}(n)$ applied to the input layer of the MLP consists of the delayed values of the output, namely, $x(n)$, $x(n\text{-}1)$, ..., $x(n\text{-}q+1)$. The output is denoted by $x(n+1)$. The dynamic behavior of the NAR model is described by

$$x(n+1) = F(x(n), x(n\text{-}1), \ldots, x(n\text{-}q+1)) \tag{3}$$

where F is a nonlinear function of its arguments, which can be approximated by MLP. The dimension and values of the input vector $\mathbf{x}(n)$ will be determined through dynamic reconstruction, which will be discussed later. Each circle shown in Figure 7 represents a neuron, and the model of it in the 1st, 2nd, and output layers can be expressed as

$$y_j^1(n+1) = \varphi\left(b_j^1(n+1) + \boldsymbol{\omega}_j^1(n+1)\mathbf{x}(n)\right) \tag{4a}$$

$$y_k^2(n+1) = \varphi\left(b_k^2(n+1) + \boldsymbol{\omega}_k^2(n+1)\mathbf{y}^1(n+1)\right) \tag{4b}$$

$$\hat{x}(n+1) = \varphi(b^{\mathrm{o}}(n+1) + \boldsymbol{\omega}^{\mathrm{o}}(n+1)\mathbf{y}^2(n+1)) \tag{4c}$$

where $\varphi(v)$ is a nonlinear activation function. Here, a logistic function given by $\varphi(v) = \frac{1}{1+\exp(-av)}$ is used. Value a is an adjustable positive parameter. Also, $\boldsymbol{\omega}_j^1(n+1)$ and $b_j^1(n+1)$ are the weight vector and bias for the j^{th} hidden node in the 1st layer, $\boldsymbol{\omega}_k^2(n+1)$ and $b_k^2(n+1)$ are the weight vector and bias for the k^{th} hidden node in the 2nd layer, and $\boldsymbol{\omega}^{\mathrm{o}}(n+1)$ and $b^{\mathrm{o}}(n+1)$ are the weight vector and bias for the node in the output layer. Vector $\mathbf{y}^1(n+1)$ consists of all node outputs in the first layer (i.e. $y_j^1(n+1)$, $j = 1, 2, \ldots, J$), and $\mathbf{y}^2(n+1)$ consists of all node outputs in the second layer (i.e. $y_k^2(n+1)$, $k = 1, 2, \ldots, K$).

In Figure 7, the prediction errors will be used for backward computation. To attain the fastest backpropagation performance, the Levenberg-Marquardt backpropagation (LM BP) algorithm is employed. The NAR network is trained to model the unknown system, which maps the input vector $\mathbf{x}(n)$ to the output $x(n+1)$, by using an open-loop NAR configuration. The trained network is then switched to a closed-loop NAR configuration for multi-step-ahead prediction so that various delays can be implemented.

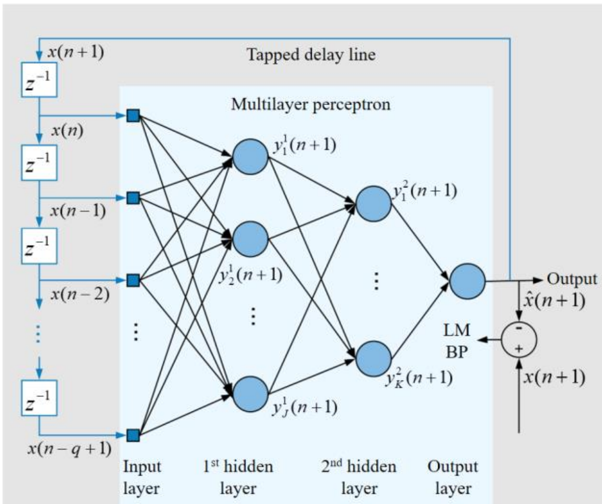

Figure 7. Architectural graph of a NAR network.

4.2.2 Dynamic Reconstruction

To identify the mapping that provides the NAR model, dynamic reconstruction is employed. The delay embedding theorem developed by Takens [43] is a fundamental result in dynamic reconstruction theory. It shows that dynamic reconstruction is possible using the m-dimensional vector $\mathbf{x}(n)$ when given the observable $x(n+1)$. The vector $\mathbf{x}(n)$ is the input vector to the input layer in Figure 7 and can be expressed as

$$\mathbf{x}(n) = [x(n), x(n\text{-}d), \ldots, x(n\text{-}(m\text{-}1)d)]^{\mathrm{T}} \quad (5)$$

where m is the embedding dimension, and d is the normalized embedding delay.

The false nearest neighbors [44] is used to estimate the embedding dimension m. By increasing m, the fraction of the false neighbors will reduce, and an appropriate embedding dimension can be determined. According to the five datasets, the explored embedding dimension is 18. The proper prescription for choosing d is to recognize that the normalized embedding delay should be large enough for $x(n)$ and $x(n\text{-}d)$ to be essentially independent of each other, but not so independent as to have no correlation with each other. This can be achieved by using the d for which the mutual information between $x(n)$ and $x(n\text{-}d)$ attains its first minimum [45]. The explored normalized embedding delay for the acquired datasets is 2. Once m and d are determined, the inputs to the MLP $\mathbf{x}(n)$ can be determined.

4.2.3 Evaluations

A root-mean-square error (RMSE) is chosen to evaluate the prediction results [46]. It can be expressed as

$$\mathrm{RMSE} = \sqrt{\frac{\sum_{i=1}^{N}\left(x(n_i) - \hat{x}(n_i)\right)^2}{N}} \quad (6)$$

where $x(n_i)$ is the desired output, $\hat{x}(n_i)$ is the actual prediction.

RMSE is a good measure of accuracy and will be used for the training data to explore the parameters (i.e. hidden layers # and neurons # in each layer) of the NAR from 12 architecture forms (Table I) by using fivefold cross-validation design. Due to the increase in complexity of the NN architecture, the computational capacity and the risk of overfitting increase. Considering this tradeoff, the explored NN architecture for the datasets is chosen to be 18-10-6-1.

With the explored NN architecture, the time delay caused by ultrasound image acquisition and processing can be compensated for. Therefore, the predicted heart position with a slow sampling rate, X_e, can be obtained.

TABLE I. NEURON NETWORK ARCHITECTURE DESIGN

No.	Architecture	No.	Architecture	No.	Architecture
1	18-6-0-1	**5**	18-10-0-1	**9**	18-14-0-1
2	18-6-3-1	**6**	18-10-3-1	**10**	18-14-3-1
3	18-6-6-1	**7**	18-10-6-1	**11**	18-14-0-1
4	18-6-9-1	**8**	18-10-9-1	**12**	18-14-3-1

*The NN architecture form indicates the number of neurons in each layer. For example, in the first architecture form, 18-6-0-1, 18 indicates the input number of the NN (explored through dynamic reconstruction), 6 and 0 indicate the neurons in the first and second hidden layers, respectively, and 1 indicates the output number of the NN.

4.3 Heart Motion Upsampling

The predicted heart position, X_e, under a lower sampling rate, ΔT, is upsampled to a higher sampling rate, Δt, by using cubic interpolation. Considering the data points, X_{e0} and X_{e1}, and assuming that n points need to be added between the two data points, a third-degree polynomial, $f(i) = ai^3 + bi^2 + ci + d$, $i \in (0, 1/(n+1), 2/(n+1), \cdots, 1)$, can be interpolated on the interval [0,1]. The four coefficients are given by

$$\begin{aligned} a &= 2f(0) - 2f(1) + f'(0) + f'(1) \\ b &= -3f(0) + 3f(1) - 2f'(0) - f'(1) \\ c &= f'(0) \\ d &= f(0) \end{aligned} \quad (7)$$

where $f(0) = X_{e0}$, $f(1) = X_{e1}$, and $f'(0)$ and $f'(1)$ are the slopes at points X_{e0} and X_{e1}.

The total time delay caused by ultrasound image acquisition and processing is approximate 160 ms. As the frame rate of the ultrasound scanner used in the paper is 25 Hz and the control frequency of the system is 1000 Hz, to compensate for the time delay of 160 ms, 4-step-ahead should be predicted in Section 4.2. In other words, to obtain X_e, D in $x(n+D)$ should be chosen as 4.

For the slave robot, the objective is to synchronize its motion with the beating heart's motion and meanwhile make the slave robot follow the position commands of the human operator. Therefore, the predicted and upsampled heart position, x_e, is added to the position of the master robot, x_m, and the summation is the desired trajectories for the slave robot, x_{ref_s} (Figure 3). Similarly, to guarantee the slave robot position, $\mathbf{x}_m$, to follow the reference trajectories, $\mathbf{x}_{ref_m}$, a PID controller is used for the slave robot. The PID controller parameters for the slave robot are $K_{p_s} = 1000$, $K_{i_s} = 0$, $K_{d_s} = 20$.

5 Experiments

5.1 *Experimental Setup*

The experimental setup (Figure 8) employs a Phantom Premium 1.5A robot (Geomagic Inc., Wilmington, MA, USA) as the master robot and a Quanser robot (Quanser Consulting Inc., Markham, ON, Canada) as the slave robot. The master and slave robots are equipped with a 50M31 force/torque sensor (JR3 Inc., Woodland, CA, USA) and a Gamma force/torque sensor (ATI Industrial Automation, Apex, NC, USA), respectively, to measure the applied interaction forces of the human operator and the beating heart.

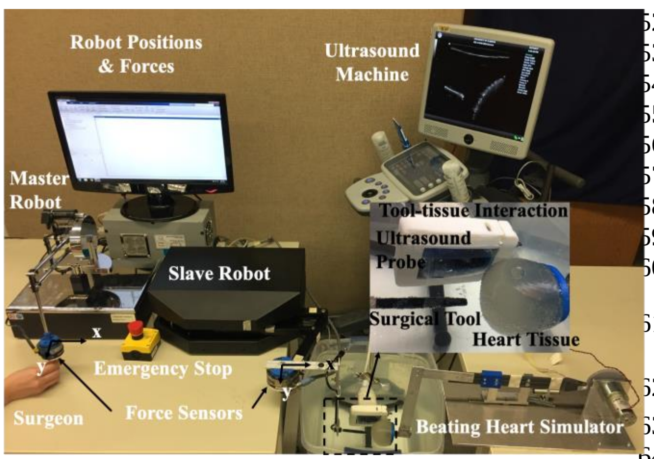

Figure 8. The experimental setup.

Table II presents the parameters used in the reference impedance model for the master robot (Equations (1) and (2)), which were obtained by trial and error during the experiments.

TABLE II. EXPERIMENTAL PARAMETERS

Symbol	*Definition*	*Value*
ω_{n_m}	Natural frequency of impedance model	0.5 rad/sec
k_m	Stiffness	4 N/m
m_m	Mass	16 kg
c_m	Damping	11.2 Ns/m
k_f	Force scaling factor	1

5.2 *Experimental Results*

To verify the advantage of the NN-based heart motion predictor, three comparative experiments are proposed: teleoperation system with master impedance control and (a) no heart motion predictor for the slave robot, (b) EKF-based heart motion predictor for the slave robot, and (c) NN-based heart motion predictor for the slave robot. In the experiments, the tested hypothesis is as follows: Motion compensation and force feedback using a NN predictor will be better than using an EKF predictor or no predictor as the NN predictor has higher accuracy and a longer prediction horizon compared to the EKF predictor or no predictor [38].

The surgical tasks in the experiments are that the human operator teleoperated a slave robot to get close to, make contact with, and break contact with the simulated beating heart tissue. During contact, the human operator is conducted to stay still so that the slave robot can primarily synchronize with the beating heart's motion. To show the difference between the three groups of experiments, in the following, only the processes of contact are presented and calculated in the results. The contact duration is defined as the time when the slave-heart tissue interaction force is greater than 0.4 N [30].

Figure 9 shows the master and slave positions and forces of the three teleoperation systems. As seen in Figure 9a, there is a significant delay (160 ms) between the positions of the slave robot and the beating heart simulator due to ultrasound image acquisition and processing. By using EKF- and NN-based heart motion predictors in teleoperation systems, this time delay is well compensated for (Figure 9b and Figure 9c). The position tracking performance of the developed system is evaluated by calculating the mean absolute synchronization error (MASE) in contact duration [25], MASE = $\frac{1}{n}\sum_{i=1}^{n}|e_i|$, where e_i is the position error between the surgical tooltip and its desired position when contact occurs, n is the sample number of contact duration. This position results are calculated and listed in Table III. The MASEs using no heart motion predictor, EKF-based predictor, and NN-based predictor are 0.0045 m, 0.0032 m, and 0.0016 m, respectively. It can be seen that using NN to predict the heart position gives the best result among the three strategies.

Additionally, in Figure 9, the forces of the master and slave robots during contact are shown. Because of the reference impedance model for the master robot, the forces perceived by the human operator are all non-oscillatory regardless of the predictor type. However, the slave-tissue interaction forces are influenced by the accuracy of heart motion compensation. The Average Forces applied by the human operator on the Master robot (AFM) and the Average Forces applied by the slave robot on the Simulated heart (AFS) for three teleoperation systems are calculated and are presented in Table III.

The standard deviations of AFM for difference heart motion predictors are small which demonstrates that good non-oscillatory force feedback is achieved. The standard deviations of AFS for the three heart motion predictors are large due to the residual mismatch between the heart motion and the slave robot motion, and due to the internal inertia of the force sensor. However, despite that, the standard deviation of AFS for NN-based predictor is smaller than that for the other predictors as the higher motion compensation accuracy. In other words, the teleoperation system with NN-based heart motion predictor can achieve the best motion compensation performance and the smallest oscillator portion of the slave-tissue interaction force among the three experimental systems. These results have tested the hypothesis that the motion compensation and force feedback using a NN predictor performs better than using an EKF predictor or no predictor for teleoperation systems in beating-heart surgery.

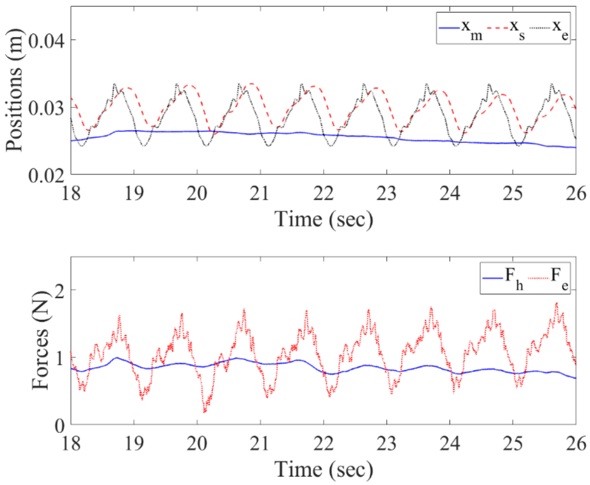

(a)

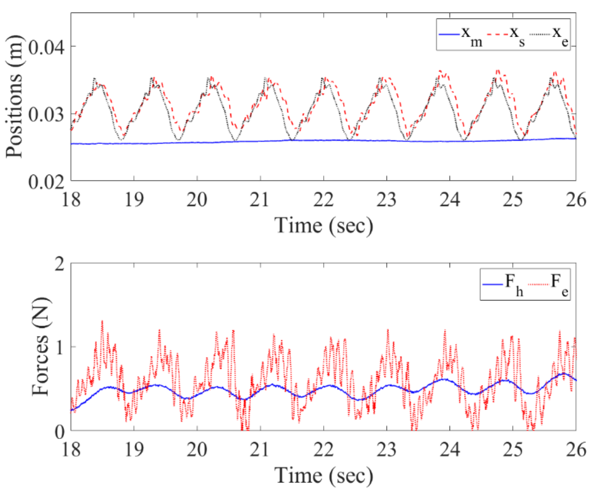

(b)

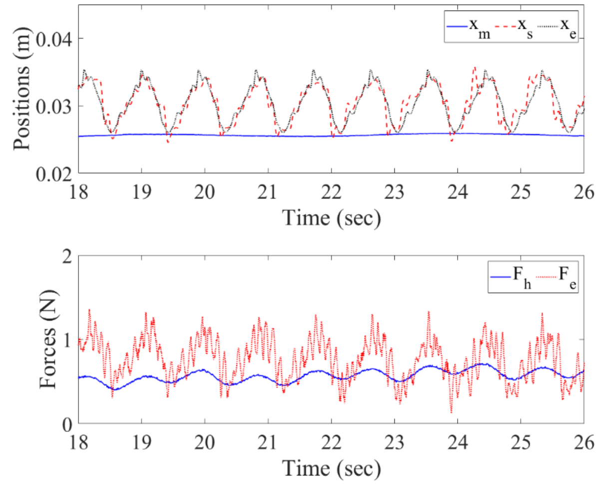

(c)

Figure 9. Position trajectories and interaction forces of the master and slave robots. Results for teleoperation system with master robot impedance control and (a) no heart motion predictor, (b) EKF-based heart motion predictor, and (c) NN-based heart motion predictor for the slave robot. In the upper position figure, the blue solid line is the position of the master robot/human operator, the red dashed line is the position of the slave robot, and the gray dotted line is the position of the heart. In the below force figure, the blue solid line is the human-master interaction force, and the red dotted line is the slave-tissue interaction force.

Table III. Experimental Results

Results	MASE (m)	AFM (N)	AFS (N)
No prediction	0.0045	0.8503 ± 0.0660	1.0568 ± 0.3282
EKF predictor	0.0032	0.4881 ± 0.0763	0.8554 ± 0.2838
NN predictor	**0.0016**	0.5674 ± 0.0679	$\mathbf{0.7622 \pm 0.2408}$

6 Conclusion

An ultrasound image-based position controller for the slave robot and an impedance controller for the master robot are proposed for a telerobotic beating-heart surgical system to simultaneously achieve heart motion compensation for the slave robot and non-oscillatory haptic feedback on the master robot. To address the time delay caused by ultrasound image acquisition and processing, a recurrent neural network is designed and treated as a heart motion predictor. The validity of the proposed teleoperation system for beating-heart surgery was verified through experiments and compared to the other two teleoperation systems without heart motion predictor and with an extended Kalman filter-based heart motion predictor. The experimental results demonstrated that the presented system with NN algorithm shows significant advantages (higher synchronization accuracy and relatively steady slave-heart contact force) over the other two systems. This shows that the proposed teleoperation system could be used in teleoperated beating heart surgeries and achieve safer and accuracy performance. In addition, the NN has great advantages over EKF on solving the heart motion prediction problem as it is more robust to unpredictive inputs such as irregular heart motion. Future work will involve exploring the system's use with surgical systems and in actual beating heart procedures.

Acknowledgement

Research supported by the Canada Foundation for Innovation (CFI) under grant LOF 28241, the Alberta Innovation and Advanced Education Ministry under Small Equipment Grant RCP-12-021, the Natural Sciences and Engineering Research Council (NSERC) of Canada under grant RGPIN 372042, the Natural Sciences and Engineering Research Council (NSERC) of Canada under grant RGPIN 03907, and the China Scholarship Council (CSC) under grant [2015]08410152.

REFERENCES

[1] *Noncommunicable Diseases Progress Monitor*. Geneva: World Health Organization, 2017.

[2] L. J. Dacey *et al.*, "Perioperative stroke and long-term survival after coronary bypass graft surgery.," *Ann. Thorac. Surg.*, vol. 79, no. 2, pp. 532–536, 2005.

[3] M. F. Newman, J. L. Kirchner, B. Phillips-Bute, *et al.*, "Longitudinal Assessment of Neurocognitive Function After Coronary-Artery Bypass Surgery," *N. Engl. J. Med.*, vol. 344, no. 6, pp. 395–402, 2001.

[4] D. Paparella, T. M. Yau, and E. Young, "Cardiopulmonary bypass induced inflammation: Pathophysiology and treatment. An update," *Eur. J. Cardio-thoracic Surg.*, vol. 21, no. 2, pp. 232–244, 2002.

[5] J. Zeitlhofer *et al.*, "Central nervous system function after cardiopulmonary bypass," *Eur. Heart J.*, vol. 14, no. 7, pp. 885–90, 1993.

[6] D. C. Bellinger *et al.*, "Developmental and neurological status of children at 4 years of age after heart surgery with hypothermic circulatory arrest or low-flow cardiopulmonary bypass," *Circulation*, vol. 100, no. 5, pp. 526–533, 1999.

[7] G. M. McKhann, M. A. Grega, L. M. Borowicz, W. A. Baumgartner, and O. A. Selnes, "Stroke and encephalopathy after cardiac surgery: An update," *Stroke*, vol. 37, no. 2, pp. 562–571, 2006.

[8] J. Fix *et al.*, "Do patients with less than 'echo-perfect' results from mitral valve repair by intraoperative echocardiography have a different outcome?" *Circulation*, vol. 88, no. 5 Pt 2. pp. II39-48, 1993.

[9] D. T. Kettler, R. D. Plowes, P. M. Novotny, N. V. Vasilyev, P. J. Del Nido, and R. D. Howe, "An active motion compensation instrument for beating heart mitral valve surgery," in *IEEE International Conference on Intelligent Robots and Systems*, 2007, pp. 1290–1295.

[10] W. Bachta, P. Renaud, E. Laroche, and J. Gangloff, "Cardiolock2: Parallel singularities for the design of an active heart stabilizer," *IEEE Int. Conf. Robot. Autom.*, 2009, pp. 3839–3844.

[11] B. Fallahi, L. Cheng, and M. Tavakoli. *State Observation and Feedback Control in Robotic Systems for Therapy and Surgery*. In Control System Design of Bio-Robotics and Bio-Mechatronic with Advanced Applications, Elsevier, 2019.

[12] M. Kitagawa, A. M. Okamura, B. T. Bethea, V. L. Gott, and W. A. Baumgartner, "Analysis of Suture Manipulation Forces for Teleoperation with Force Feedback," in *5th International Conference on Medical Image Computing and Computer Assisted Intervention*, 2002, pp. 155–162.

[13] M. Tavakoli, A. Aziminejad, R. V. Patel, and M. Moallem, "High-fidelity bilateral teleoperation systems and the effect of multimodal haptics," *IEEE Trans. Syst. Man, Cybern. Part B*, vol. 37, no. 6, pp. 1512–1528, 2007.

[14] K. J. Kuchenbecker and G. Niemeyer, "Induced Master Motion in Force-Reflecting Teleoperation," *J. Dyn. Syst. Meas. Control*, vol. 128, no. 4, pp. 800–810, 2006.

[15] R. A. MacLachlan, B. C. Becker, J. C. Tabarés, G. W. Podnar, L. A. Lobes, and C. N. Riviere, "Micron: An actively stabilized handheld tool for microsurgery," *IEEE Trans. Robot.*, vol. 28, no. 1, pp. 195–212, 2012.

[16] Y. Nakamura, K. Kishi, and H. Kawakami, "Heartbeat synchronization for robotic cardiac surgery," *IEEE Int. Conf. Robot. Autom.*, vol. 2, pp. 2014–2019, 2001.

[17] R. Ginhoux, J. Gangloff, M. de Mathelin, L. Soler, M. M. Arenas Sanchez, and J. Marescaux, "Active filtering of physiological motion in robotized surgery using predictive control," *IEEE Trans. Robot.*, vol. 21, no. 1, pp. 67–79, 2005.

[18] A. Schweikard, G. Glosser, M. Bodduluri, M. J. Murphy, and J. R. Adler, "Robotic Motion Compensation for Respiratory Movement During Radiosurgery," *Comput. Aided Surg.*, vol. 5, pp. 263–277, 2000.

[19] S. G. Yuen, D. T. Kettler, P. M. Novotny, R. D. Plowes, and R. D. Howe, "Robotic motion compensation for beating heart intracardiac curgery," *Int. J. Rob. Res.*, vol. 28, no. 10, pp. 1355–1372, 2009.

[20] S. G. Yuen, S. B. Kesner, N. V Vasilyev, P. J. Del Nido, and D. Howe, "3D Ultrasound-Guided Motion Compensation System for Beating Heart Mitral Valve Repair," *Med. Image Comput. Comput. Interv.*, vol. 11, no. Pt 1, pp. 711–719, 2008.

[21] S. B. Kesner and R. D. Howe, "Robotic catheter cardiac ablation combining ultrasound guidance and force control," *Int. J. Rob. Res.*, vol. 33, no. 4, pp. 631–644, 2014.

[22] M. Bowthorpe and M. Tavakoli, "Physiological organ motion prediction and compensation based on multirate, delayed, and unregistered measurements in robot-assisted surgery and therapy," *IEEE/ASME Trans. Mechatronics*, vol. 21, no. 2, pp. 900–911, 2016.

[23] M. Bowthorpe and M. Tavakoli, "Ultrasound-Based Image Guidance and Motion Compensating Control for Robot-Assisted Beating-Heart Surgery," *J. Med. Robot. Res.*, vol. 1, no. 1, p. 1640002, 2016.

[24] M. Bowthorpe and M. Tavakoli, "Generalized Predictive Control of a Surgical Robot for Beating-heart Surgery Under Delayed and Slowly-sampled Ultrasound Image Data," *IEEE Robot. Autom. Lett.*, vol. 1, no. 2, pp. 892–899, 2016.

[25] L. Cheng and M. Tavakoli, "Ultrasound image guidance and robot impedance control for beating-heart surgery," *Control Eng. Pract.*, vol. 81, pp. 9–17, 2018.

[26] P. Moreira, N. Zemiti, C. Liu, and P. Poignet, "Viscoelastic model based force control for soft tissue interaction and its application in physiological motion compensation," *Comput. Methods Programs Biomed.*, vol. 116, no. 2, pp. 52–67, 2014.

[27] R. Cortesão and M. Dominici, "Robot Force Control on a Beating Heart," *IEEE/ASME Trans. Mechatronics*, vol. 22, no. 4, pp. 1736–1743, 2017.

[28] E. E. Tuna, T. J. Franke, O. Bebek, A. Shiose, K. Fukamachi, and M. C. Cavuşoğlu, "Heart Motion Prediction Based on Adaptive Estimation Algorithms for Robotic Assisted Beating Heart Surgery," *IEEE Trans. Robot.*, vol. 29, no. 1, pp. 261–276, 2013.

[29] Ö. Bebek and M. C. Çavusoglu, "Intelligent Control Algorithms for Robotic-Assisted Beating Heart Surgery," *IEEE Trans. Robot.*, vol. 23, no. 3, pp. 468–480, 2007.

[30] L. Cheng, M. Sharifi, and M. Tavakoli, "Towards Robot-Assisted Anchor Deployment in Beating-Heart Mitral Valve Surgery," *Int. J. Med. Robot. Comput. Assist. Surg.*, vol. 14, no. 3, p. e1900, 2018.

[31] L. Cheng and M. Tavakoli, "Switched-Impedance Control of Surgical Robots in Teleoperated Beating-Heart Surgery," *J. Med. Robot. Res.*, pp. 1841003, 2018.

[32] L. Cheng, J. Fong, and M. Tavakoli, "Semi-Autonomous Surgical Robot Control for Beating-Heart Surgery," in *IEEE 15th International Conference on Automation Science and Engineering*, pp. 1774-1781, 2019.

[33] L. Guo, N. Li, F. Jia, Y. Lei, and J. Lin, "Neurocomputing A recurrent neural network based health indicator for remaining useful life prediction of bearings," *Neurocomputing*, vol. 240, pp. 98–109, 2017.

[34] J. Tang, F. Liu, Y. Zou, W. Zhang, and Y. Wang, "An Improved Fuzzy Neural Network for Traffic Speed Prediction Considering," *IEEE Transactions on Intelligent Transportation Systems*, vol. 18, no. 9, pp. 2340–2350, 2017.

[35] I. Bukovsky *et al.*, "A Fast Neural Network Approach to Predict Lung Tumor Motion during Respiration for Radiation Therapy Applications," *Biomed Res. Int.*, pp. 489679(1–13), 2015.

[36] T. P. Teo *et al.*, "Feasibility of predicting tumor motion using online data acquired during treatment and a generalized neural network

optimized with of fl ine patient tumor trajectories," *Am. Assoc. Phys. Med.*, vol. 45, no. 2, pp. 830–845, 2018.

[37] V. De Luca *et al.*, "Evaluation of 2D and 3D ultrasound tracking algorithms and impact on ultrasound-guided liver radiotherapy margins," *Am. Assoc. Phys. Med.*, vol. 45, no. 11, pp. 4986–5003, 2018.

[38] L. Cheng and M. Tavakoli, "Neural - Network - Based Heart Motion Prediction for Ultrasound - Guided Beating - Heart Surgery," in *IEEE 15th International Conference on Automation Science and Engineering*, 2019.

[39] M. Sharifi, H. Salarieh, S. Behzadipour, and M. Tavakoli, "Beating-heart robotic surgery using bilateral impedance control: Theory and experiments," *Biomed. Signal Process. Control*, vol. 45, pp. 256–266, 2018.

[40] M. Bowthorpe, V. Castonguay-siu, and M. Tavakoli, "Development of a Robotic System to Enable Beating-heart Surgery," *J. Robot. Soc. Japan*, vol. 32, no. 4, pp. 23–30, 2014.

[41] I. Sobel, "An isotropic 3 by 3 image gradient operator," *Mach. Vis. three-demensional Sci.*, vol. 1, no. 1, pp. 23–34, 1990.

[42] R. O. Duda and P. E. Hart, "Use of the Hough transform to detect lines and cures in pictures," *Commun. Assoc. Comput. Mach.*, vol. 15, no. 1, pp. 11–15, 1972.

[43] F. Takens, "On the numerical determination of the dimension of an attractor," *Dynamical systems and bifurcations*, Springer, Berlin, Heidelberg, pp. 99-106, 1985.

[44] H. Abarbanel. *Analysis of oberserved chaotic data*. Springer Science & Business Media, 2012.

[45] A. M. Fraser, "Information and Entropy in Strange Attractors," *IEEE Trans. Inf. Theory*, vol. 35, no. 2, pp. 245–262, 1989.

[46] N. K. Ahmed, A. F. Atiya, N. El Gayar, and H. EI-Shishiny, "An Empirical Comparison of Machine Learning Models for Time Series Forecasting," *Econometric Reviews*, vol. 29, no. 5, pp. 594-621, 2010.